Available online at www.sciencedirect.com
SCIENCE DIRECT®
Journal of Sound and Vibration 270 (2004) 259–278
JOURNAL OF SOUND AND VIBRATION
www.elsevier.com/locate/jsvi

Spectral quality of acoustic predictions obtained by the ray method in coupled two-dimensional damped cavities ☆

T. Courtois[a], V. Martin[b,*]

[a] *Rieter Automotive France SA, F-78140 Aubergenville, France*
[b] *Electromagnetism and Acoustics Laboratory, Swiss Federal Institute of Technology, CH-1015 Lausanne, Switzerland*

Received 20 March 2002; accepted 14 January 2003

Abstract

Numerical modelling of coupling in acoustics in the medium-frequency range poses problems, which remain to be solved. Indeed, in such cases, finite element methods in volumes or on boundaries generate too large a number of degrees of freedom due to the size of the domains (the volumes or the boundaries). With the ray method in simple convex damped cavities, it is possible to target a small number of points inside the domain and, subsequently, to economize on calculation time, making it possible to look for spectral instead of harmonic results. Does this still hold when damped cavities are coupled by an acoustic transmission path or by a vibrating structure, with aural perception in view? In fact, due to inherent approximations, the ray method is inaccurate in the presence of absorbent walls and thus in damped coupled cavities. However, an analysis will show that a hierarchy exists among the errors arising from the rays, and finally it will appear that only the grazing rays must be replaced by another approximation. In these conditions, the ray method is capable of solving coupling problems in acoustics in the medium-frequency range with greater computing speed than finite element methods.

1. Introduction

One method for solving harmonic linear acoustic problems consists in using the integral representation of the Helmholtz equation. The easiest case is when certain simple integrals, the so-called single layer, are to be calculated. To this end, the Green kernel must satisfy some boundary conditions of the problem under study. Unfortunately, such an elementary function

☆ At its start, the project was carried out at the Laboratoire de Mécanique de Rouen, CNRS-INSA de Rouen, F-76801 Saint Etienne du Rouvray, France, where both authors worked.

*Corresponding author.
E-mail addresses: tcourtoi@insa-rouen.fr (T. Courtois), vincent.martin@epfl.ch (V. Martin).

0022-460X/03/$ - see front matter © 2003 Elsevier Ltd. All rights reserved.
doi:10.1016/S0022-460X(03)00493-0

(the Green function) is rarely known analytically, if only because of the geometry of the domain concerned. In the low-frequency range such a kernel has already been built by the finite element method, but this method is inadequate when dealing with medium frequencies. It was thus decided to use the image source method to obtain the Green function. Correlatively, the notion of specular reflection with its associated reflection coefficient is accepted, although it is inaccurate within the framework of the differential equations of linear acoustics. However, the errors induced are important only for a limited number of rays from among all those necessary to build the solution. With this remark in mind, it is worth asking if this method might not provide an acceptable kernel for our purpose, i.e., to predict acoustic pressure in the medium-frequency range, with aural perception in view. In other words, the question answered in this paper is: what are the consequences of the approximations inherent to the ray method on the solution of a problem with a certain degree of complexity? The motivation of the present study originates from the coupling of two damped cavities, similar to those encountered in a car.

The comparison of the present approach with that made by other authors requires some technical explanations which constitute the first part of the presentation, followed by the geometrical configuration which is at the origin of the work: two acoustic cavities coupled by an interface. The global approach to the problem, by integral representation as well as the rays present at each step is then given. Section 4 recalls the specular reflection and the next section presents the directivity, emphasizing its validity for the terms necessary for the calculation used in the global approach. It will then appear that the grazing ray between source and receiver located quite near each other on the same plane wall, is responsible for the greatest error and must be replaced by another more appropriate approximation. In Section 7, an account is provided of the numerical experiments carried out to observe the influence of the approximations on the final results of a coupling problem. The reference solution comes from the finite element method as the particular configuration chosen has a sufficiently small number of degrees of freedom. The present study not only emphasizes the nature of the approximations inherent to the ray method but also gives an idea of their hierarchy, as far as errors are concerned. Spectral synthesis in thirds of octaves will show that the results obtained are quite acceptable when predictions are for aural perception in the sense of perceived sound level (binaural perception, usually more concerned with source localization, is sensitive to the interaural time differences added to diffractions around the head and a more precise frequency scale probably ought to be chosen).

Finally, the paper shows that despite the absence of a rigorous method to carry out acoustic coupling of damped cavities in the medium-frequency range, it is nevertheless possible to obtain reasonably good results through the Green functions built by the ray method, still bearing in mind its weaknesses. The proposed approach extends to damped non-convex domains seen as coupled damped convex domains by identity transfer at the interfaces.

2. Considerations regarding the choice of the Green function

Flow charts followed by calculations to solve dynamic coupling problems in linear elastic media were at the centre of a work published some years ago [1]. Where acoustics is concerned, the operators are either in differential or integral forms. The latter case is attractive as it transforms a domain problem into a contour problem that, in certain situations, makes resolution easier. We

are concerned here only with the direct integral representation solved most often by the collocation technique [2]. Mastering the global procedure and having chosen an integral representation, the Green kernel(s) remain(s) to be chosen, in particular in the medium-frequency range, given our objectives.

It is well known that solving a problem using the integral representation implies two parts: one associated with the elementary solution chosen and the other consisting of a correction in the form of contour integrals. A judicious choice of the kernel limits the correction to be made by reducing the contour where the modifications occur and/or by working only with this simple the so-called single layer term.

Only very particular geometries and boundary conditions lead to elementary solutions available in analytical form, such as the closed-form solution, modal series or ray series, the coefficients of which have a simple analytical expression. Keeping as close as possible to our preoccupation, let us quote the paper of Lam and Hodgson [3] who deal with the radiation of a vibrating body located inside a rectangular enclosure with absorbent walls. Here, the Green function is written as a series of rays which satisfy the enclosure boundary conditions. This results in correction only on the boundary of the vibrating body, but with double and single layer terms. Let us note that the vibrating body is transparent to the rays of the elementary solution leading to some approximations made only on the walls of the enclosure. More precisely, of the three approximations shown in the present paper, only the specular reflection need be considered.

Except in the very few cases of particular geometries and boundary conditions, the Green function may be obtained using numerical methods. When looking for a procedure to optimize absorbent device locations on the wall of an enclosure, the Green function leaving only single layer terms in the correction was built by the finite element method [4]. As already mentioned, this method is inappropriate for the medium-frequency range, because it would lead to a very large number of degrees of freedom inside the domain or on the contour. A ray method is a better choice in this frequency range. It can give information at a small number of points, making it possible to save calculation time and memory size, and subsequently to predict whole spectra at a few points instead of the whole field for one frequency. In complex geometries, the solution originating from a series of rays is numerical as it derives from an algorithm. Closest to our problem of damped cavities in the medium-frequency range written through an integral representation, the kernel of which is built by a ray method, one has to mention the work of Jean [5] focussing on the radiation of a source inside an enclosure. The walls are equipped with damped materials except one or a part of one made up of a vibrating panel, the velocity of which is given, i.e., here without coupling. The elementary solution chosen here satisfies the same boundary conditions where the walls are damped and a condition of rigid wall where it would otherwise vibrate. The correction is then only on the yielding wall with just one single layer term. Let us mention that the absence of coupling removes the grazing ray intervening in coupled cavities.

Although our configuration is different, if only due to the coupling, a particular point of the method quoted above could have been followed a priori. However, at the very beginning of our work, we opted for the Green functions that, in each of the two coupled cavities, satisfy the boundary conditions of the problem except on the sides of the interface where they satisfy boundary conditions of the same nature as those on the damped walls. The choice of this option resulted from two imperatives: to limit the number of rays in building the elementary functions and, above all, to reduce as far as possible, one of the errors inherent to the ray method. Indeed,

let us consider only one damped cavity with a yielding wall on its contour. The kernel leading to a single layer on the yielding wall may satisfy a rigid boundary condition there as seen above, or also an absorbing condition. In fact, the building of the kernel by rays requires an approximation which turns out to be quite good when the vibrating wall is large and has the same type of boundary condition as those of the other parts of the contour. Correlatively a small vibrating surface with rigid behaviour in the midst of damped material is an unfavourable case. Moreover, choosing a Green function with an impedance relation on the vibrating wall of the same nature as that on the other part of the contour, the number of rays will also remain relatively small as, for the kernel, the cavity is totally damped. For two coupled cavities, the same arguments hold, replacing the vibrating wall with the sides of the interface.

3. Configuration of coupled acoustic cavities and general procedure

3.1. Configuration

The question of the relevance of building a Green function by the geometrical method for a coupled problem originated from the automobile field where noise generated in the cavity which houses the engine radiates towards the passengers cabin through the dashboard. The generic configuration is given in Fig. 1. Fig. 2 shows the geometry of the two cavities used to illustrate the case numerically. They are of identical shape to save memory size and computation time when using the finite element method to obtain the so-called reference solution. There is thus a geometrical symmetry around the wall containing the interface. The damping acoustic behaviour of boundaries $\partial\Omega_1$ and $\partial\Omega_2$ (which do not include the faces of the interface) is modelled with local reaction through the impedance. Indeed, for harmonic acoustic fields, the reduced impedance is defined by $Z_r = \mathbf{p}/\rho c\mathbf{v}_n$, where $\mathbf{p}$ and $\mathbf{v}_n$ are, respectively, the acoustic pressure and the normal acoustic velocity, with the normal on the boundary directed inwards from the domain, and ρc the characteristic impedance of the air. This definition inserted into the dynamic equation of Euler leads to the following relation satisfied at the boundaries:

$$\nabla\mathbf{p}\cdot\mathbf{n} = -\frac{ik}{Z_r}\mathbf{p}. \tag{1}$$

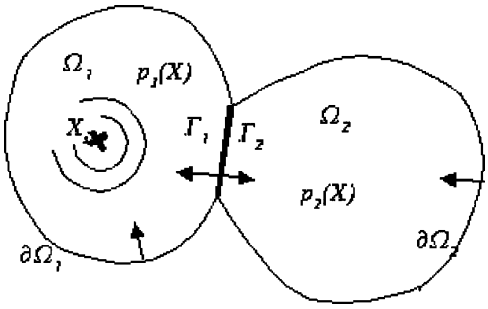

Fig. 1. Two acoustic cavities Ω_1 and Ω_2 are coupled by an interface Γ, with sides Γ_1 and Γ_2.

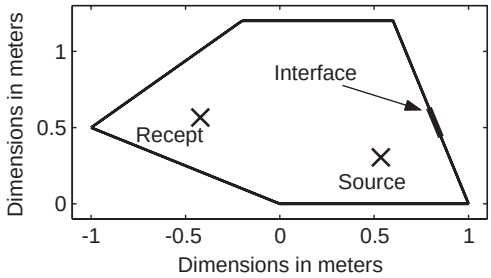

Fig. 2. Both cavities have the same shape to save computation size when seeking the reference solution.

A point source velocity is located inside Ω_1 at $\mathbf{x}_S$. It is expected that the transfer through the interface modifies the responses of the isolated cavities. The problem can be solved globally—i.e., without subdomain considerations or, in other words, without the use of substructures—in which case, the finite element method could provide the reference solution. The same solution with the same method can also be obtained from substructure analysis when considering each domain separately. With such a procedure the finite element method built up the Green function of each domain in the way mentioned before. As already written, this procedure cannot be extended to the medium-frequency range, for technical rather than conceptual reasons, which is why the solution is sought by the ray method with integral representation, here only written on either side of the interface.

3.2. General procedure

General flow charts associated with coupling problems in elastic media have been widely described [1], so will only be outlined here. The method used is the boundary integral method where the Green kernels in each cavity are such that only single layer terms intervene on the contours.

The whole domain is made up of three media: two cavities Ω_1 and Ω_2 and the interface Γ with its sides Γ_1 and Γ_2 seen from Ω_1 and Ω_2, respectively. The goal is to determine the acoustic pressure in each cavity, given the source in Ω_1.

The behaviour of the interface is described through a transfer matrix such that

$$\begin{Bmatrix} \mathbf{p}_2(\Gamma_2) \\ \mathbf{v}_{2n}(\Gamma_2) \end{Bmatrix} = \begin{bmatrix} T_{11} & T_{12} \\ T_{21} & T_{22} \end{bmatrix} \begin{Bmatrix} \mathbf{p}_1(\Gamma_1) \\ \mathbf{v}_{1n}(\Gamma_1) \end{Bmatrix},$$

which links the acoustic pressures and normal velocities on each side. When sides Γ_1 and Γ_2 are discretized into facets, the quantities $\mathbf{p}(\Gamma)$ and $\mathbf{v}_n(\Gamma)$ must be understood as vectors the components of which are the values of p and v_n on each facet.

Let us suppose that, in Ω_1, the solution $G_1(\mathbf{x},\mathbf{x}')$ which satisfies

$$\begin{cases} H_{\mathbf{x}} G_1(\mathbf{x},\mathbf{x}') = -\delta(\mathbf{x}-\mathbf{x}') & \text{in } \Omega_1, \\ G_{1,n_{\mathbf{x}}} + \mathrm{i}k\beta_1 G_1 = 0 & \text{on } \partial\Omega_1 \cup \Gamma_1 \end{cases}$$

is known, where $H_{\mathbf{x}}$ is the Helmholtz differential operator with the space variable $\mathbf{x}$ and where $G_{1,n_{\mathbf{x}}}$ is the normal derivative of $G_1(\mathbf{x},\mathbf{x}')$ at point $\mathbf{x}$ on the boundary of Ω_1 (the boundary of Ω_1 is

made up of $\partial\Omega_1 \cup \Gamma_1$). For generality, the source is supposed to be extended on the boundary of $\Omega_S \subset \Omega_1$ and to appear in the right-hand member of the Helmholtz equation as $f(\mathbf{x})$. So, when $\mathbf{x} \in \Omega_1 \backslash \Omega_S$, defining the admittance $\beta_1 = 1/Z_{r_1}$, the integral representation of the Helmholtz operator results in

$$p_1(\mathbf{x}) = -\int_{\Omega_S} G_1(\mathbf{x},\mathbf{x}')f(\mathbf{x}')\,\mathrm{d}\mathbf{x}' + \mathrm{i}\rho\omega \int_{\Gamma_1} G_1(\mathbf{x},\mathbf{x}')v_{1n}(\mathbf{x}')\,\mathrm{d}\mathbf{x}' - \mathrm{i}k\beta_1 \int_{\Gamma_1} G_1(\mathbf{x},\mathbf{x}')\,p_1(\mathbf{x}')\,\mathrm{d}\mathbf{x}'. \quad (2)$$

Before reaching $\mathbf{p}_1$ in Ω_1 both quantities $\mathbf{p}_1$ and $\mathbf{v}_{1n}$ have to be determined first on Γ_1. The discretization into facets of Γ_1 leads classically to the matricial form

$$[\mathbf{A}_1]\{\mathbf{p}_1(\Gamma_1)\} = \{\mathbf{f}_1\} + [\mathbf{B}_1]\{\mathbf{v}_{1n}(\Gamma_1)\}.$$

In Ω_2 we define $\mathbf{G}_2(\mathbf{x},\mathbf{x}')$ which satisfies

$$\begin{cases} H_{\mathbf{x}} G_2(\mathbf{x},\mathbf{x}') = -\delta(\mathbf{x}-\mathbf{x}') & \text{in } \Omega_2, \\ G_{2,n_{\mathbf{x}}} + \mathrm{i}k\beta_2 G_2 = 0 & \text{on } \partial\Omega_2 \cup \Gamma_2 \end{cases}$$

with the above notations. Here also, the contour of Ω_2 is made up of $\partial\Omega_2 \cup \Gamma_2$. For $\mathbf{x} \in \Omega_2$, the integral representation is

$$p_2(\mathbf{x}) = +\mathrm{i}\rho\omega \int_{\Gamma_2} G_2(\mathbf{x},\mathbf{x}')v_{2n}(\mathbf{x}')\,\mathrm{d}\mathbf{x}' - \mathrm{i}k\beta_2 \int_{\Gamma_1} G_2(\mathbf{x},\mathbf{x}')\,p_2(\mathbf{x}')\,\mathrm{d}\mathbf{x}' \quad (3)$$

with its corresponding matrix equation

$$[\mathbf{A}_2]\{\mathbf{p}_2(\Gamma_2)\} = [\mathbf{B}_2]\{\mathbf{v}_{2n}(\Gamma_2)\}.$$

From the matrix forms above, follows the system of four matrix equations for four unknown vectors which must be solved to obtain the pression in Ω_1 as well as in Ω_2 :

$$\begin{bmatrix} \mathbf{A}_1 & \mathbf{0} & -\mathbf{B}_1 & \mathbf{0} \\ \mathbf{0} & \mathbf{A}_2 & \mathbf{0} & -\mathbf{B}_2 \\ \mathbf{T}_{11} & -\mathbf{I} & \mathbf{T}_{12} & \mathbf{0} \\ \mathbf{T}_{21} & \mathbf{0} & \mathbf{T}_{22} & -\mathbf{I} \end{bmatrix} \begin{Bmatrix} \mathbf{p}_1(\Gamma_1) \\ \mathbf{p}_2(\Gamma_2) \\ \mathbf{v}_{1n}(\Gamma_1) \\ \mathbf{v}_{2n}(\Gamma_2) \end{Bmatrix} = \begin{Bmatrix} \mathbf{f}_1 \\ \mathbf{0} \\ \mathbf{0} \\ \mathbf{0} \end{Bmatrix}.$$

3.3. Rays present in each integral

The building of both kernels G_1 and G_2 requires here the image source method and thus rays. The various types of rays needed to calculate each of the integrals are enumerated.

Let us work first with integral $\int_{\Omega_S} G_1(\mathbf{x},\mathbf{x}')f(\mathbf{x}')\,\mathrm{d}\mathbf{x}'$, where $\Omega_S \subset \Omega_1$ and $\mathbf{x} \in \Omega_1$, $\mathbf{x}$ outside Ω_S. A point source at $\mathbf{x}_S$ would result in $G_1(\mathbf{x},\mathbf{x}_S)f_S$, a quantity homogeneous to a pressure $q(\mathbf{x})$. In geometrical acoustics, $q(\mathbf{x})$ stems from a direct ray travelling from the source at $\mathbf{x}_S$ towards the receiver at $\mathbf{x}$, and also from all the rays reflected on the walls, arising from the image sources, all outside the convex domain. Despite the inaccurate notion of specular reflection in the presence of absorbent walls, Section 4 will show that the approximation of $q(\mathbf{x})$ by the image source method, in other words the construction of $G_1(\mathbf{x},\mathbf{x}_S)$ by rays, is quite acceptable as long as the source and the receiver are sufficiently distant from the boundaries. This remark applies to all point sources $\mathbf{x}'$ in the volume integral.

Concerning the contour integrals, several situations appear. With the discretization of side Γ_1 of the interface into facets Γ_{1i}, the so-called collocation calculation uses the following approximation: $\int_{\Gamma_1} G_1(\mathbf{x},\mathbf{x}')h(\mathbf{x}')\,d\mathbf{x}' \simeq \sum_i h(\mathbf{x}_i)\int_{\Gamma_{1i}} G_1(\mathbf{x},\mathbf{x}')\,d\mathbf{x}'$. When the receiver is located at $\mathbf{x}\in\Omega_1$, the source at $\mathbf{x}'$ now radiating from the wall, $G_1(\mathbf{x},\mathbf{x}')$ consists of the direct ray travelling from $\mathbf{x}'$ towards $\mathbf{x}$ and of the reflected rays emitted from the image sources of $\mathbf{x}'$ against the walls. As long as the receiver is sufficiently far from the wall Γ_1 where the source $\mathbf{x}'$ is located, the rays give a good approximation (Section 5). At this stage in our procedure, a remark should be made. Whatever the image source, the ray reaching the receiver originates from the source $\mathbf{x}'$ on the wall. In the case of a large number of image sources, many rays leave the source $\mathbf{x}'$ on the wall to reach, after a certain number of reflections, the receiver. It could occur that an image source might be located on the prolongation of a wall, but in that case only a small number of rays emitted by that image source would illuminate the receiver and thus participate in the global radiated pressure. In other words, the particularity due to the fact that $\mathbf{x}'$ is located on a wall cannot be ignored, while that same particularity will not be taken into consideration for very few rays radiated from very few image sources also on walls, on account of their negligible contribution to the global result.

When the receiver is closer to the wall Γ_1, the previous approximation is no longer acceptable. This unfortunately is what will occur in the process of determining $\mathbf{p}_1$ and $\mathbf{v}_{1n}$ on Γ_1 before calculating $\mathbf{p}_1$ in Ω_1 since, in that process, $\mathbf{x}\in\Gamma_1$. When discretizing into facets, a distinction is usually made between the case where $\mathbf{x}\notin\Gamma_{1i}$ in $\int_{\Gamma_{1i}} G_1(\mathbf{x},\mathbf{x}')\,d\mathbf{x}'$ and the case where $\mathbf{x}\in\Gamma_{1i}$. The first term is called term of interinfluence on Γ_1, the second of autoinfluence on Γ_1, the latter existing as a Cauchy integral. Presently, in both cases, $G_1(\mathbf{x},\mathbf{x}')$ results from a grazing ray travelling from $\mathbf{x}'$ towards $\mathbf{x}$ and also from rays radiated from the image sources of $\mathbf{x}'$ against the walls. This grazing ray is *the* ray with such an error and with such a great influence on the final result that a substitute must be found (Section 6). Here again an important remark regarding the procedure chosen should be made. The grazing ray from $\mathbf{x}'$ towards $\mathbf{x}$ travels a short distance, in particular in the autoinfluence terms. It could occur by geometrical chance that an image source might be located on the prolongation of the same wall, thus also radiating a grazing ray. However, in such a case, the image source would be quite far from the receiver, and this grazing ray could be ignored because, as it will be shown, its contribution to the total result is insignificant. Everything that has been said for $G_1(\mathbf{x},\mathbf{x}')$ on Γ_1 is obviously true for $G_2(\mathbf{x},\mathbf{x}')$ on Γ_2.

The present work intends to emphasize the approximations inherent to some rays and which subsequently lead to errors in some integrals, keeping in mind the objective of aural perception, and eventually binaural perception [6]. However, the intention is not to make a thorough analysis of each case encountered but to show their influence on global calculations in a coupled cavities configuration, where a large number of rays intervene, the majority of them being "regular".

4. Approximations due to geometry and specular reflection

In general, geometrical acoustic methods are not intended for examining the acoustic field everywhere in a cavity domain (only convex cavities are envisaged here; non-convex cavities come into the framework of coupled cavities). Instead, knowing the source and making the choice of hearing point(s), a selection is carried out within the space and the acoustic spectrum is synthesized from the main contributing rays at the hearing point(s). Two types of approximation

are inherent to these methods. Errors arise from the geometrical building of rays and their impacts on the boundaries, as well as from the way the boundary conditions are considered.

Let us work with an omnidirectional source radiating a spherical wave. To take into account the numerous reflections on the walls, the wave front is discretized. The description of the propagation from source to receiver is two-fold [7]. On the one hand, the whole wave front is propagated through discretization with a large number of cones, each around a central ray with a probability of reaching the receiver. Only the central ray is considered and not the cone cross-section itself. This procedure is called ray tracing. Various approximations arise from the cone size: for instance, in the description of the intensity distribution in the cone and in the influence of the impacts on cavity vertices and edges. The use of the wave front is easily accepted intuitively. On the other hand, propagation paths between source and receiver are identified through the notion of image sources S_j [8]. The ray bears the propagation. With this approach, chosen with our end in view, the geometrical approximations disappear. The complexity of the rapid selection of image sources "seen" from the receiver(s) grows with the complexity of the geometry. Vorländer [9] has devised an algorithm of selection by using data from ray tracing. The technique used here, not developed in the present paper, is an extension that establishes "visible" image source families by a process related to the lighting of the cavity by the successive image sources.

Having adopted a geometrical method, convergence towards the exact solution is now expected when the number of "useful" rays increases. However, this is impossible with absorbent walls from a rigorous point of view. Is this an obstacle? The method consists in transforming a problem in a bounded domain into a sum of problems in the unbounded domain. For the sake of simplicity, let us work in the two-dimensional space (2D). The wave, harmonic, is cylindrical. The image source S_j radiates the pressure

$$\mathbf{p}(r_j) = f_j \frac{-\mathrm{i}}{4} H_0^-(kr_j),$$

where r_j is the distance from the image source at $\mathbf{x}_j$ to the hearing point at $\mathbf{x}$, k the wave number, H_0^- the Hankel function of zero order. The term f_j will be related to the image source later on. With the N_S first image sources, the pressure obtained at the receiver at $\mathbf{x}$ is

$$\mathbf{p}(\mathbf{x}) = \frac{-\mathrm{i}}{4} \sum_{j=1}^{N_S} f_j H_0^-(kr_j).$$

The contribution $\mathbf{p}(r_j)$ of each ray has an amplitude and a phase which reveal not only the propagation path but also the damping behaviour of the walls. The complex part of a reflected wave has been determined analytically in the past by various authors [10,11]. This cornerstone of the present discussion will be shown in a simple way and will not be analyzed as deeply as in the references quoted.

Reflected acoustic pressure p_{ref} depends on the incident pressure p_{inc} via a reflection coefficient R such that $p_{ref} = Rp_{inc}$. Given the damping acoustic behaviour of the walls through a local reaction, coefficient R is derived by noting that relation (1) satisfied for each ray contributing to the pressure is also satisfied for the sum of the rays. Moreover, the contribution of one ray, written p_{ray}, at the wall is a local sum made up of the incident and the reflected pressures

or $p_{ray} = p_{inc} + p_{ref}$. Thus an R such that $p_{ref} = Rp_{inc}$ at $\mathbf{x}$ on the boundary must satisfy (1) with

$$\partial_n p_{inc}(\mathbf{x}) + \partial_n p_{ref}(\mathbf{x}) = -\frac{ik}{Z_r}(p_{inc}(\mathbf{x}) + p_{ref}(\mathbf{x})).$$

This description of the reflection qualified as specular leads to modelling errors. It is true that in the case of a square domain with perfectly rigid walls, it has been verified that the solution of the acoustic differential equations obtained by the modal theory or the finite element method, and that obtained with the geometrical method are the same [12]. However, the differences between the two solutions increase when the walls have a reactive behaviour (the impedance has an imaginary part) and especially when the form of the cavity is irregular. Is it therefore possible to define the validity domain of the specular reflection ? To this end, one ray is isolated by working in the half-space, the boundary of which is of constant impedance value. Fig. 3 gives the configuration. The operator is as follows:

$$\begin{cases} H_{\mathbf{x}} p(\mathbf{x}) = -f\,\delta(\mathbf{x} - \mathbf{x}_s) \quad \text{with } \mathbf{x} \in \Omega, \\ \partial_n p(\mathbf{x}) = -\dfrac{ik}{Z_r} p(\mathbf{x}) \quad \text{for } \mathbf{x} \in \Gamma, \\ \text{radiation at infinity.} \end{cases} \tag{4}$$

The wave radiated by an omnidirectional 2D point source is cylindrical. Acoustic pressure is made up of a direct field $p_{dir}(\mathbf{x})$ and a reflected field $p_{ref}(\mathbf{x})$. The direct field is obtained by the Green function $g(\mathbf{x},\mathbf{x}_S)$ of the unbounded space while the reflected field has to be determined

$$p(\mathbf{x}) = p_{dir}(\mathbf{x}) + p_{ref}(\mathbf{x}).$$

Concerning the specular reflection, precision can be increased by writing

$$p_{refl}^{spec}(\mathbf{x}) = R(\mathbf{x}_P, \theta) g(\mathbf{x}, \mathbf{x}'_s),$$

where $\mathbf{x}_P$ is the impact point of the direct ray on the boundary, $\mathbf{x}'_S$ the image source location, θ the angle of incidence of the direct ray on the boundary. The dependence of the pressure on $\mathbf{x}$ (and also on the source location $\mathbf{x}_S$) is coherent with the impact point and the incidence angle resulting from the receiver and the image source locations, i.e., from the source co-ordinates. In the present situation where a cylindrical wave impinges to the boundary, the dynamic equation at the origin

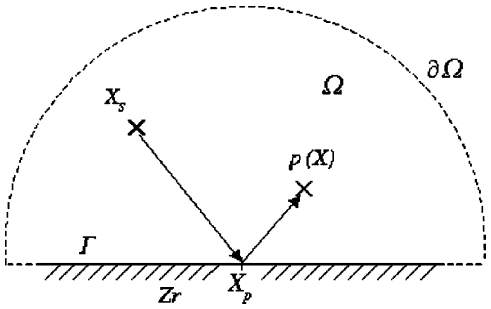

Fig. 3. In half-space, only one reflection occurs in the solution.

of (1) also leads to

$$R_{cyl} = \frac{Z_r \cos\theta \frac{H_1(k|\mathbf{x}\text{-}\mathbf{x}_S|)}{\mathrm{i}H_0(k|\mathbf{x}\text{-}\mathbf{x}_S|)} - 1}{Z_r \cos\theta \frac{H_1(k|\mathbf{x}\text{-}\mathbf{x}_S|)}{\mathrm{i}H_0(k|\mathbf{x}\text{-}\mathbf{x}_S|)} + 1}. \tag{5}$$

The exact solution of operator (4) satisfies the integral representation of the Helmholtz equation

$$p^{ex}_{ref}(\mathbf{x}) = g(\mathbf{x}, \mathbf{x}'_S) - 2\frac{\mathrm{i}k}{Z_r}\int_\Gamma g(\mathbf{x}, \mathbf{x}')p(\mathbf{x}')\,\mathrm{d}\mathbf{x}'.$$

The field reflected is thus due to the totally reflected incident wave corrected by a sum of scattered waves on the whole damped boundary. In fact, it is known that in the latter term, the contribution of the far part of the boundary is negligible.

The above equation makes it possible to quantify the approximation inherent to the specular reflection. Indeed, let us write

$$p^{ex}_{refl}(\mathbf{x}) = R_{id}(\mathbf{x})g(\mathbf{x}, \mathbf{x}'_s),$$

where $R_{id}(\mathbf{x})$ is identified from the exact solution leading to

$$R_{id}(\mathbf{x}) = 1 - 2\frac{\mathrm{i}k}{Z_r}\frac{\int_\Gamma g(\mathbf{x}, \mathbf{x}')p(\mathbf{x}')\,\mathrm{d}\mathbf{x}'}{g(\mathbf{x}, \mathbf{x}'_s)}. \tag{6}$$

Comparison between $R(\mathbf{x}_P, \theta)$ and the true value $R_{id}(\mathbf{x})$ gives the answer sought. Fig. 4 presents the configuration where the spatial dimensions are normalized versus the wavelength λ to be free of frequencies (i.e., the space variable is $\gamma = r/\lambda$). Fig. 5 shows the discrepancies, i.e., the modelling errors when working with the specular reflection coefficient. As a rule of thumb, the reflected field is far from the specular reflection for oblique incidences when the receiving point is near the wall ($\gamma_R \to 0$), and the difference decreases as the distance grows (in other words as the frequency increases). This phenomenon has long been observed. More quantitavely, the specular reflection induces significant errors for a distance of less than one wavelength as far as real impedances are concerned. In that case the error is less than 12% for incidences less than 60°. Fig. 5 emphasizes the detrimental influence of the reactive part of the impedance, essentially when looking at the phase due to the reflection. It has been verified that this influence grows when the imaginary part of the impedance increases. When going beyond this distance of one wavelength, these phase errors diminish. It is not easy to go further in error quantification as the influence of the impedance reactive part does not seem to vary according to any simple rule.

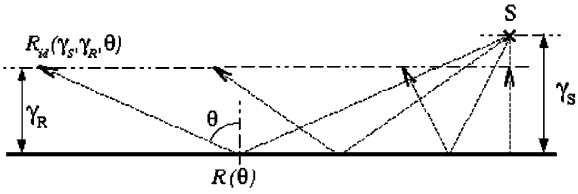

Fig. 4. Coefficient R_{id} results from the exact value of the reflected field, at a constant adimensional distance γ from the wall, according to the incidence of the rays, ranging from 0° to 85°. The source at one wavelength from the wall is at the adimensional distance $\gamma_S = 1$.

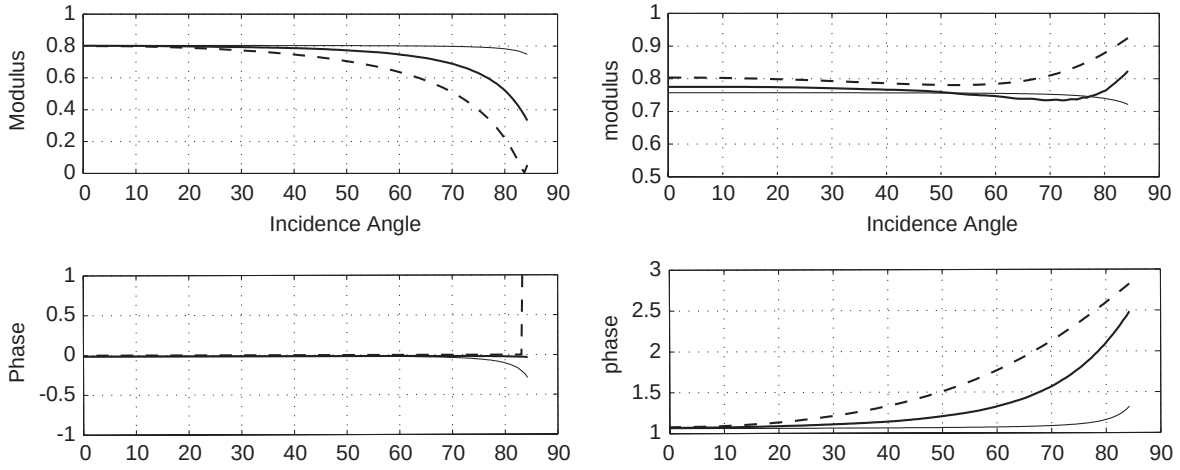

Fig. 5. Comparison between modulus and phases of the specular reflection coefficient R (– – –) and the identified reflection coefficient R_{id} at a distance from the wall of one wavelength (———) and of 0.1 wavelength (——); graphs on the left for the impedance value of 9; graphs on the right for the impedance value of 0.4 (1.+ i4.).

The coefficient R associated with the specular reflexion gives access to the reflected pressure p_{ref} as long as $\mathbf{x}_S$ and $\mathbf{x}_R$ are located inside the domain Ω. For the impedance values considered, from among all the rays satisfying the configuration, those with θ greater than 70° are largely erroneous, the others being acceptable. Now, when $\mathbf{x}_S$ belongs to the boundary, $\mathbf{x}_R$ still being inside Ω, coefficient R lacks sense except for the plane wave. Unfortunately, in the vicinity of a point source (or lineic in 2D), the plane wave has no physical reality and, morover, p_{ref} also lacks sense. What model can therefore describe the configuration?

5. Radiation of sources on walls

The previous section focused on sources (including the image sources) far from the boundaries. That is not the only case dealt with in this study. The influence of the interface through the integral $\int_{\Gamma_{1,2}} G_{1,2}(\mathbf{x}, \mathbf{x}')\,\mathrm{d}\mathbf{x}'$ is also calculated taking into consideration point sources on either side Γ_1 and Γ_2 of interface Γ. Section 3.2 emphasized that the Green functions $G_{1,2}(\mathbf{x}, \mathbf{x}')$, each associated with a domain isolated, satisfy an impedance relation at the interface, which is different from the radiation at infinity and from the perfectly rigid reflection.

Here, within the framework of geometrical methods in acoustics, the problem of radiation in the half-space of a source located at $\mathbf{x}_S$ on the boundary, the impedance of which is of constant value, is studied as a generic problem to gauge the approximations. As in the previous section, source and receiver first keep their functions, but it will be shown later that here the reciprocity has an interesting role to play. Let us thus suppose that the field radiated at a receiver depends continuously on the source location when it tends towards the wall from inside the domain, i.e., when the distance, r_s decreases ($r_S \to 0$). This hypothesis makes it possible to extend the specular reflection of Section 4 again in a simple way, without any deep analytical insight. Here incident and reflected waves are no longer the correct words. Instead, the field $p(\mathbf{x})$ is broken down into the

direct component $p_{dir}(\mathbf{x})$, which does not recognize the existence of the boundary, and the correction $p_{corr}(\mathbf{x})$ due the boundary. Of course, the direct contribution arises from the Green function $g(\mathbf{x}, \mathbf{x}_S)$ of the unbounded space. The other component can be assimilated to a reflection with the form $p_{corr}(\mathbf{x}) = R(\mathbf{x}_P, \theta) \cdot g(\mathbf{x}, \mathbf{x}'_S)$, where $|\mathbf{x}_S - \mathbf{x}'_S| \to 0$ and $|\mathbf{x}_P - \mathbf{x}_S| \to 0$ since the source, its image and the impact on the wall merge at the limit, resulting in

$$p_{corr}(\mathbf{x}) = \lim_{r \to 0} R(\theta, r) \cdot g(\mathbf{x}, \mathbf{x}_S).$$

The solution thus takes the form $p(\mathbf{x}) = (1 + \lim_{r \to 0} R(\theta, r)) g(\mathbf{x}, \mathbf{x}_S)$ written

$$p(\mathbf{x}) = D(\theta) g(\mathbf{x}, \mathbf{x}_S)$$

by defining $D(\theta)$, the specular directivity of the source on the wall. In the present situation, the directivity could have been properly defined, if the cylindrical reflection coefficient R_{cyl} had been meaningful at the wall. Instead, the plane wave approximation at the wall is accepted as leading to the specular directivity

$$D(\theta) = 1 + R_{pl} = 2 \frac{Z_r \cos\theta}{1 + Z_r \cos\theta}. \tag{7}$$

The problem under study has an exact solution, with which the specular directivity is compared. The integral representation of the Helmholtz equation with the source at the wall is

$$p^{ex}(\mathbf{x}) = 2g(\mathbf{x}, \mathbf{x}_S) - 2 \frac{\mathrm{i}k}{Z_r} \int_\Gamma g(\mathbf{x}, \mathbf{x}') p(\mathbf{x}') \, \mathrm{d}\mathbf{x}'.$$

According to this exact solution, the boundary effect cannot be qualified by only a local directivity since the above equation shows a scattering from the whole boundary in the second term on the right-hand side. As before, the exact solution gives an identified directivity coefficient now compared with the specular directivity. Let us note $p^{ex}(\mathbf{x}) = D_{id}(\mathbf{x}) g(\mathbf{x}, \mathbf{x}_S)$ with

$$D_{id}(\mathbf{x}) = 2 - 2 \frac{\mathrm{i}k}{Z_r} \frac{\int_\Gamma g(\mathbf{x}, \mathbf{x}') p(\mathbf{x}') \, \mathrm{d}\mathbf{x}'}{g(\mathbf{x}, \mathbf{x}_S)}. \tag{8}$$

The numerical comparison is carried out with the spatial dimension reduced to the wavelength. The source at the walls leads to $\gamma_S = 0$. Fig. 6 presents the results for two values of γ (at the receiver) and for incidences from 0° to 85°. The farther the receiver from the wall and the higher the frequency, the more accurate the approximation. It is very efficient at the distance of one wavelength from the wall for incidences ranging from 0° to 80°, here for real as well as for complex impedances; however, the error is greater for large imaginary parts in the impedance. For a real impedance, the approximation is worthwhile even at one-tenth of the wavelength as the error is less than 10% for incidences less than 60°.

In half-space the specular directivity is truly satisfactory. Surprisingly, it gives better results than the specular reflection. Until now no explanation has been found for this unexpected quality. However, noticing that coefficient R leads to the total pressure p via p_{ref} while coefficient D leads directly to p, the remark above could suggest that the exact contribution of p_{dir}, the pressure due to the direct ray, on p is more important than the erroneous contribution arising from R when $\mathbf{x}_S$ is located on the boundary.

In a cavity, the comparison using the reciprocity principle gives another reason for accepting the approximation of the specular directivity. Indeed, the transfer between a point $\mathbf{x}$ inside the

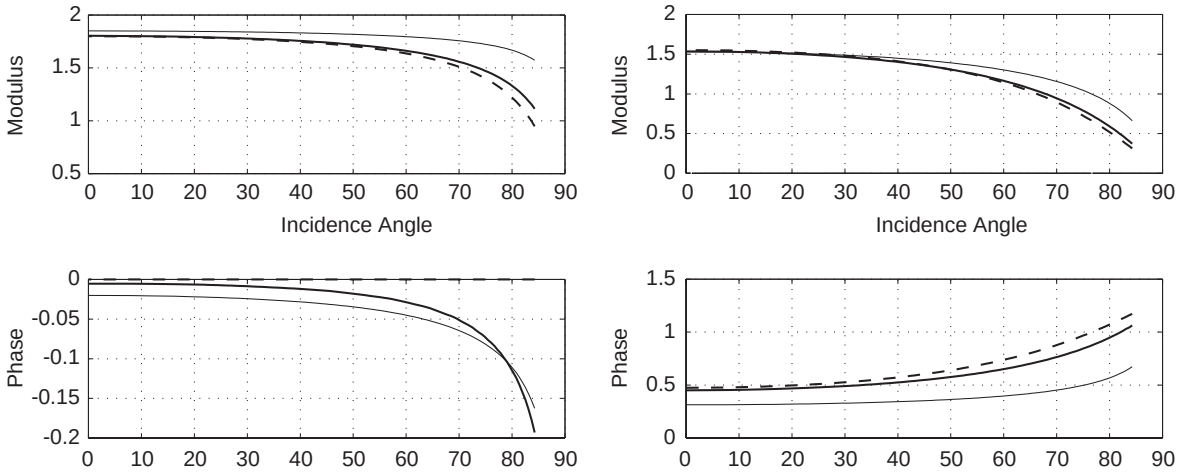

Fig. 6. Comparison between modulus and phases of specular directivity coefficient D (– – –) and the identified directivity coefficient D_{id} at a distance from the wall of one wavelength (———) and of 0.1 wavelength (——); graphs on the left for the impedance value of 9; graphs on the right for the impedance value of 0.4 (1. + i4.).

domain and a point $\mathbf{x}'$ on the boundary is identical with $G(\mathbf{x}, \mathbf{x}')$ or $G(\mathbf{x}', \mathbf{x})$. In the numerical experiment, the transfer function stems from the geometrical method using one of the two following procedures:

- the hearing point is on the wall while the omnidirectional source is at $\mathbf{x}$ inside the cavity; the result of the experiment is $G(\mathbf{x}', \mathbf{x})$, working with all the image sources of $\mathbf{x}$ and
- the source $\mathbf{x}'$ is on the wall and the hearing point in the domain; the source with its specular directivity and the image sources with the specular reflection approximation lead to $G(\mathbf{x}, \mathbf{x}')$.

The walls are of real or complex impedance. Fig. 7 shows that both geometrical solutions are identical. For curiosity's sake, Fig. 7 also gives the amplitude of the pressure inside the domain when the source is on the wall, but without taking into account the specular directivity. This reciprocity experiment results in the specular directivity not bringing supplementary errors to the solution obtained from the numerous reflected rays and conversely. Such a conclusion makes it possible to reduce considerably the calculations needed to obtain the influence of the wall on the receiver. Indeed, when $\mathbf{x}'$ varies on Γ, for each $\mathbf{x}'$ the calculation of its image sources must be carried out and then the field calculated at the receiver $\mathbf{x}$ in Ω. When the source $\mathbf{x}$ in Ω is given, the image sources have to be calculated only once and then the field calculated at each $\mathbf{x}'$ on Γ. The precision of the numerical value of the integral $\int_\Gamma G_{1,2}(\mathbf{x}, \mathbf{x}')\,\mathrm{d}\mathbf{x}'$ depends on its discretization on $\Gamma_{1,2}$ and on the number of integration points. The work is thus carried out with all integration points as receivers.

This section has thus shown that, with a source located on the absorbent boundary and the receiver inside the domain, reciprocity gives the same results as those obtained with specular directivity, the latter being understood as the limit of the specular reflection when the source inside the domain tends towards the boundary. Provided some hypotheses are made, in particular about angle θ, the approximation of the directivity can be accepted. For practical reasons of computation speed, reciprocity will be used here.

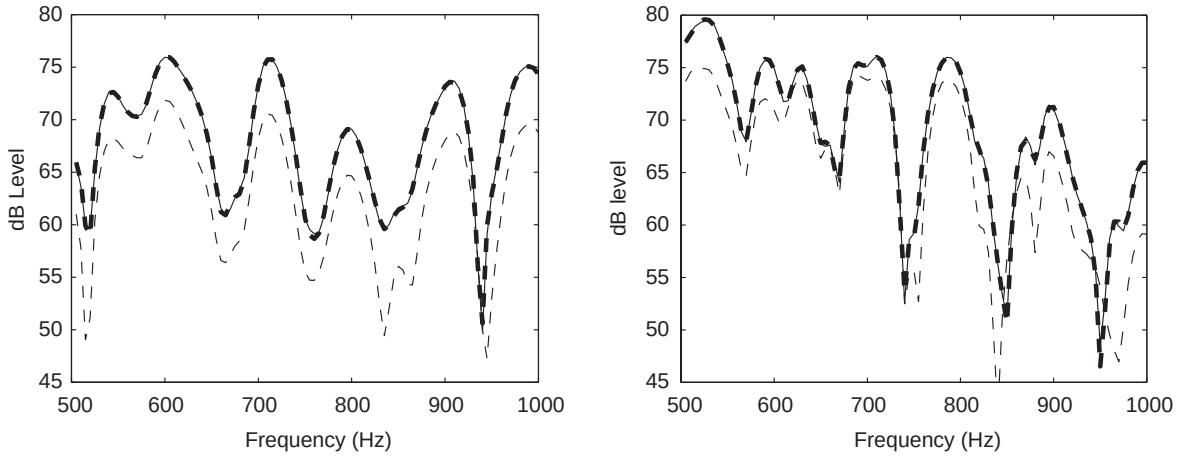

Fig. 7. Reciprocity of responses between one point on the wall and another inside the cavity. Spectra results from the source on the wall and the receiver in the domain with (——) and without (– – –) the directivity coefficient, and from the same points, with roles inverted (– – –). The points coordinates in Fig. 2 are (−0.733 0.733) on the wall and (0.547, 0.313) inside the domain.

6. The grazing ray in the contour integrands

It has been shown that a wall source radiating not very far by a ray, the incidence of which is greater than 80° approximately, leads to a large error in the predicted pressure at a receiver within the domain. The error increases with the incidence. What then can be expected from the terms of inter- and autoinfluence present in the coupling problem dealt with here? Indeed they are of the form $\int_{\Gamma_{1,2}} G_{1,2}(\mathbf{x},\mathbf{x}')\,\mathrm{d}\mathbf{x}'$, where $\mathbf{x}$ is also on $\Gamma_{1,2}$ and the grazing ray of the Green kernel is unavoidable.

Could it be possible to exploit the directivity coefficient already introduced? Let us note that $\lim_{\theta\to 90^\circ} D(\theta) = 0$. If this limit had been exact, it would have led to a zero contribution of the grazing ray, while this is far from being the case when source and receiver are not very far apart. More precisely, let us consider two points $\mathbf{x}$ and $\mathbf{x}_S$ located on the absorbent wall of the infinite half-space. The exact pressure results from the integral representation, written with the Green function of the infinite space $g(\mathbf{x},\mathbf{x}')$. Indeed the pressure at $\mathbf{x}$ on the boundary is expressed by

$$p^{ex}(\mathbf{x}) = 2g(\mathbf{x},\mathbf{x}_S) - 2\frac{\mathrm{i}k}{Z_r}\int_{\Gamma} p(\mathbf{x}')g(\mathbf{x},\mathbf{x}')\,\mathrm{d}\mathbf{x}'.$$

Points $\mathbf{x}'$ on Γ distant from $\mathbf{x}$ hardly contribute to the final value and the discretization on a finite part of Γ leads to

$$p^{ex}(\mathbf{x}) \simeq 2g(\mathbf{x},\mathbf{x}_S) - 2\frac{\mathrm{i}k}{Z_r}\cdot\sum_j p(\mathbf{x}_j)\int_{\Gamma_j} g(\mathbf{x},\mathbf{x}')\,\mathrm{d}\mathbf{x}'.$$

The usual calculations result in the value of $p^{ex}(\mathbf{x})$ due to a source at $\mathbf{x}_S$. Writing this pressure $p^{ex}(d,Z_r)$ to emphasize that it depends on the distance $d = |\mathbf{x}-\mathbf{x}_S|$ and on the impedance Z_r, and introducing an identified the so-called emission coefficient $M_{id}(d,Z_r)$ such that

$p^{ex}(d, Z_r) = M_{id}(d, Z_r)g(d)$, i.e.,

$$M_{id}(d, Z_r) \simeq 2 - 2\frac{ik}{Z_r}\frac{\sum_j p(\mathbf{x}_j)\int_{\Gamma_j} g(\mathbf{x}, \mathbf{x}')\,d\mathbf{x}'}{g(\mathbf{x}, \mathbf{x}_S)}, \tag{9}$$

it becomes possible to compare $M_{id}(d, Z_r)$ with the directivity coefficient $D(\theta)$ for $\theta = 90°$, i.e., zero. Fig. 8 shows the emission coefficient for a real and a complex value of Z_r against the normalized distance $\gamma = d/\lambda$. It appears that $\lim_{\gamma\to 0} M_{id}(\gamma, Z_r) = 2$ and $\lim_{\gamma\to\infty} M_{id}(\gamma, Z_r) = 0$. Thus, the limit value of zero for the directivity coefficient has a sense only for the receiver located far from the source on the boundary. Fig. 8 also shows the rate of decrease to zero for $M_{id}(\gamma, Z_r)$, which depends on wall impedance and frequency. In those conditions, and given the a posteriori (but expected) importance of the grazing ray in the final result of our problem, there was no choice but to find an alternative to evaluating the inter- and autoinfluence integrals. Until now, the grazing ray has been replaced by the exact value of the pressure radiated at a receiver by a source, both on the boundary of an infinite half-space. A database taking into account the impedance of the boundary, the distance between source and receiver and the frequency, must thus be made before the coupling problem can be solved. The information is gathered in a vector consisting of the emission coefficient $M_{id}(\gamma, Z_r)$ and, as written previously, the contribution of the grazing ray at adimensional distance is $p^{ex}(\gamma, Z_r) = M_{id}(\gamma, Z_r)g(\gamma)$. For the autoinfluence where the Cauchy integral derives from an analytical calculation, the multiplicative coefficient is the emission coefficient.

The direct ray in a cavity where the walls are of finite dimensions is not of exactly the same nature as that occurring on the infinite boundary of a half-space. However, a numerical experiment where both source and receiver are on the same wall shows that the use of the latter

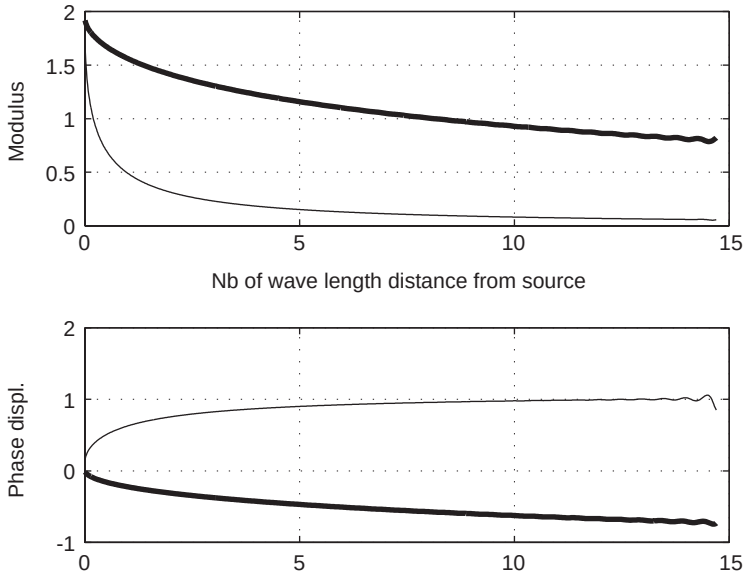

Fig. 8. Modulus and phases of the ratio of the wall pressure to the pressure in the infinite medium, according to the distance to the source, for two impedance values: $Z_r = 9$ (———) and $Z_r = 0.4(1. + i4.)$ (——).

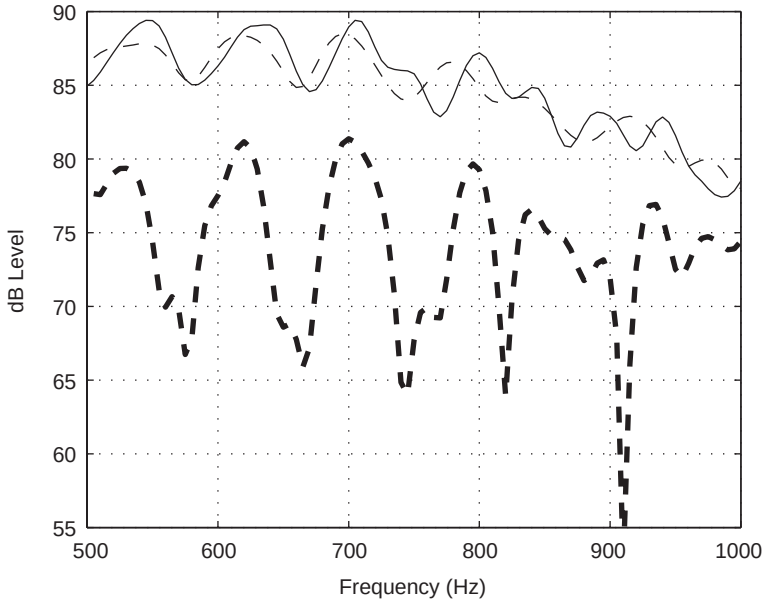

Fig. 9. Spectra of the responses from a source to a receiver on the same wall, 0.04 m apart: comparison between the geometrical (– – –) and the finite element solutions (——). Without the grazing ray (– – –), the spectrum is not acceptable.

solution greatly improves the result. In the test carried out in the cavity of Fig. 2, the distance between source and receiver is voluntarily short ($d = 0.04$ m). The contribution of the direct or grazing ray is extracted from the database, and the contribution of the other rays is obtained from the specular reflection model, valid for a very large majority of them. In the very particular case where one image source would be located on the prolongation of the boundary containing $\mathbf{x}$ and $\mathbf{x}'$, another grazing ray would occur. However, the image source far from the receiver contributes nothing to the result. In Fig. 9, three graphs present three ways of calculating the "pressure" $G_1(\mathbf{x},\mathbf{x}')$: the reference solution obtained using the finite element method, and the geometrical solutions with and without the grazing ray (as defined in the half-space). The importance of this ray appears fully here. The procedure proposed is of limited efficiency, essentially for walls with complex impedances, but it nevertheless improves the result significantly, and will therefore be used for approaching the contour integrals. How will this influence the final prediction?

7. Consequences of ray approximations on prediction in coupled cavities

The problem under study is described in Section 2. Acoustic pressure predictions result from the Green functions G_1 and G_2 built with the geometrical method, i.e., with image sources and their corresponding rays. The previous sections have shown why this approach is not rigorous and made us aware of the errors accompanying some of the rays incorporated in the Green functions. Given the numerous rays taken into account in solving the problem, do the errors on some of

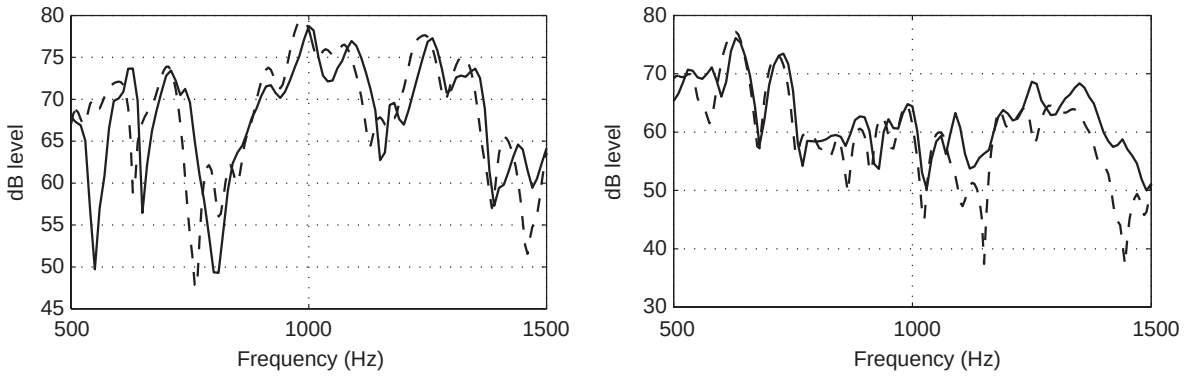

Fig. 10. Sound level in each of the coupled cavities: comparison of the levels obtained by the ray (– – –) and finite element (——) methods, for real impedance values of 9.

them affect the final result ? The reference solution comes from the finite element method in the medium-frequency range. The source is located in Ω_1. The radiated pressures are observed at two points R_1 and R_2, each in a cavity. The simplest transfer matrix, the identity, reveals the continuity of the pressures and of the normal velocities at the interface. The cavities' boundaries, outside the faces of the interface, are of the same impedance value.

In the first numerical experiment, the cavity boundaries reflect a large amount of the incident pressures with a real impedance value of 9. Fig. 10 compares the predicted spectra at points R_1 and R_2, with the reference solution. In this case, where the spectra show large fluctuations according to frequency, the trends remain. However, for frequencies between 500 and 800 Hz at point R_1 and between 1000 and 1150 Hz, for example, at point R_2 the difference is more visible than elsewhere. It could be that the points chosen simply happen to be the worst. To have another idea of the quality of the results, Fig. 11 shows the comparison between the phases at a point on the interface for the approximated ray method and the reference method. Indeed, we learned during the numerical experiments that the results at the interface master the solution inside the domains and that the phase plays an important role. Both curves show the same trends.

Fig. 10 could seem to indicate that the mean level is respected but not the fluctuations. By increasing the damping at the boundaries, still with a real impedance, less fluctuations are expected. Graphs of Fig. 12 result from an impedance value of 3, equivalent to an absorption coefficient of 0.75 for a normal incidence. In fact, the predicted spectra are in good agreement with those of reference as the discrepancies are quite always below 2 dB. Going further into the dependence of the results on the impedance value, the numerical tests are now inspired by the case of materials encountered in cars. It is known that their reactive part increases as the frequency decreases. In the frequency range of interest the imaginary part of the impedance is quite high. In Fig. 13 results show again that large fluctuations of the spectra are not well described by the approximation method, but that the trends are still present.

The above comparisons have been given in very narrow frequency bands. However, the question of the validity of the ray method in the medium-frequency range applies to hearing, which is why Fig. 14 presents the results of Fig. 13, not the best obtained, by thirds of octave frequency bands. The differences are of 2 dB at most. This constitutes our conclusion since it provides an affirmative answer to the question asked in the introduction.

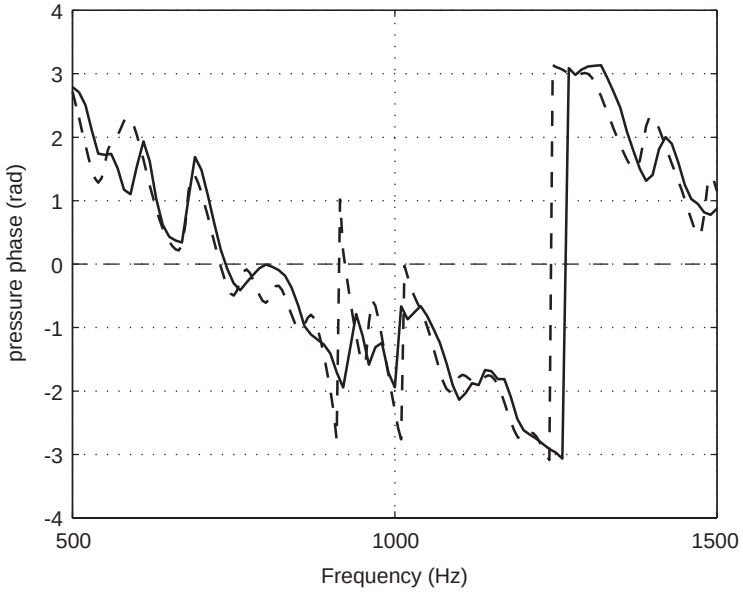

Fig. 11. Comparison between the pressure phases at the interface according to frequency, obtained by the geometrical (– – –) and the finite element (——) methods, for the impedance value of 9.

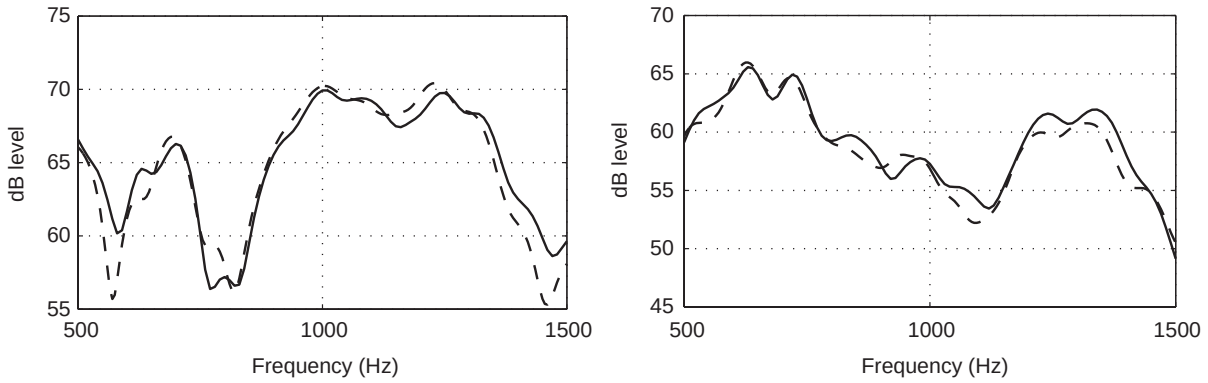

Fig. 12. Sound level in each of the coupled cavities: comparison of the levels obtained by the ray (– – –) and finite element (——) methods, for high damping due to the real impedance value of 3.

8. Conclusion

The question asked concerns the consequences on predictive calculations of the approximations associated with the geometrical methods used in acoustic coupling problems for medium frequencies, with aural perception considerations in view. The answer brought by the paper is the following: from among the configurations tested, the poorest results lead to a difference of 2 dB between the spectrum obtained by the ray method and the spectrum obtained by a reference method, the spectra being understood in thirds of octaves for frequencies from 500 to 1600 Hz. It

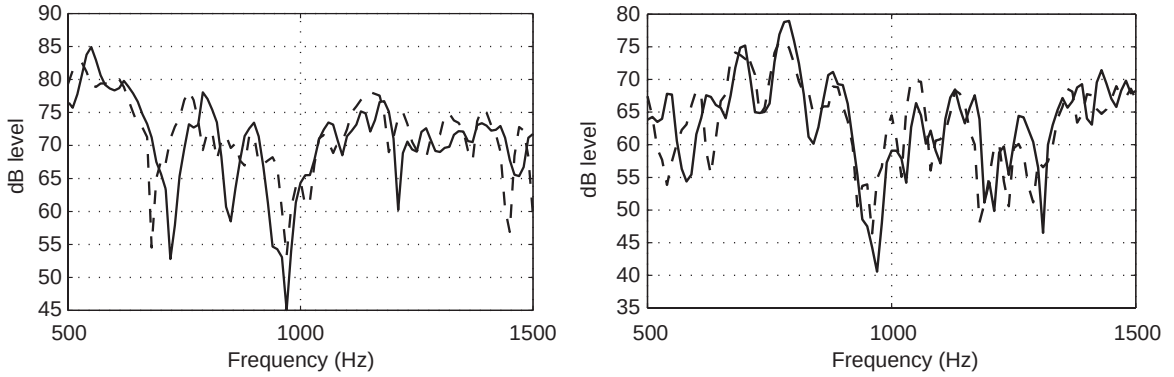

Fig. 13. Sound level in each of the coupled cavities: comparison of the levels obtained by the ray (– – –) and finite element (——) methods, for a complex impedance value of 0.4(1. + i4.).

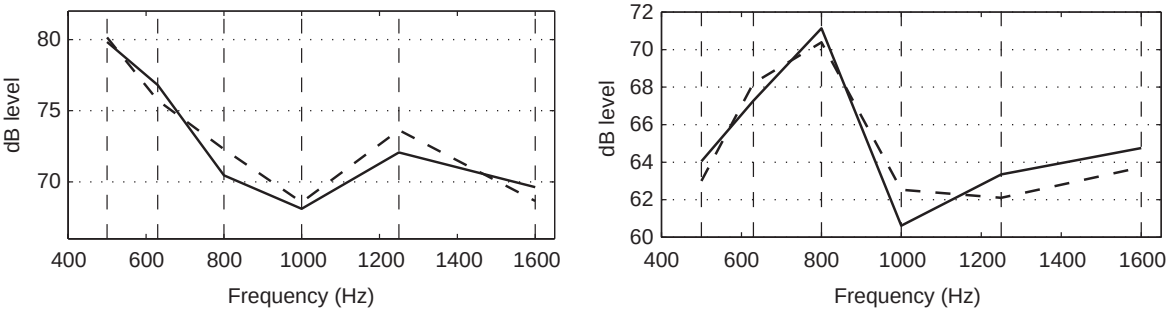

Fig. 14. Sound level in each of the coupled cavities: comparison of the levels in thirds of octaves obtained by the ray (– – –) and finite element (——) methods, for a complex impedance value of 0.4(1. + i4.).

should certainly not be taken for granted that this would always be the case, but it has been shown that such results are possible. It has also to be noted that these results can be further improved where the walls are of weak reactive acoustic behaviour.

To obtain these performances, a major difficulty was removed in each cavity. This was the grazing ray present in the inter and autoinfluence terms of the integral representation of the coupling problem, representation that is said to be simplified because the Green kernel is built to remove the double layer terms, leaving only the single layer terms. Indeed the grazing ray on the interfaces is too far from satisfying the validity conditions of the specular reflection to be acceptable, which is why a table of values obtained from the boundary of a half-space with the same absorption as that of each side of the interface, i.e., as that of each cavity boundary, replaces the grazing ray.

As for the validity domain of the specular reflection associated with the image source method, it varies according to the point source located inside one of the coupled domains or on the interface, the point of reception being inside the domain that "sees" the point source. When the source is inside, the specular reflection model is quite sufficient noting that high frequencies, real impedances and weak incidences are the most favourable cases, properties which have long been

well known. When the source is on one side of the interface, a directivity model applied to the direct ray results in a very acceptable solution for incidences less than 80° (the simple form given to the directivity is a model as it leads to information in good agreement with a physical intuition, despite the legitimate criticism about the plane wave). However, this remark is not definitive as the solution depends on the frequency and on the value of the interface impedance. In general, short wavelengths and real impedances are favourable. Nevertheless, it has emerged that the directivity model for rays arising from sources on the interface is very appropriate for the present objectives.

To sum up, by describing the procedure chosen in such a way as to highlight its advantages and drawbacks, the quantification of the approximations made when considering the specular reflection, the directivity model and the grazing rays, has identified the latter as the cornerstone of geometrical methods in coupling problems. As soon as $\mathbf{x}$ and $\mathbf{x}'$ in $G(\mathbf{x},\mathbf{x}')$ are located on the interface, the grazing ray must be taken into account and this is inevitable when coupling is really present. This difficulty being removed thanks to an erstaz, the global approach has proved to be capable of dealing with complex problems in the medium-frequency range. Let us note that the approach proposed could also be used to deal with non-convex domains. Indeed, within the framework of this paper, they can be seen as coupled convex domains with identity interfaces. In three-dimensional space, computation is also very rapid. The coupling experiment, currently being carried out, is expected to play the role played here by the numerical solution of reference obtained by the finite element method.

References

[1] V. Martin, B. Peseux, Flow chart for numerical coupling of dynamic problems in elastic media, *International Journal for Numerical Methods in Engineering* 37 (1994) 4285–4308.

[2] D.T.I. Francis, M.M. Sadek, An integral equation method for predicting acoustic emission within enclosures, *Journal of Mechanical Engineering Science, Part C* 199 (1985) 133–137.

[3] Y.W. Lam, D.C. Hodgson, The prediction of the sound field to an arbitrary vibrating body in a rectangular enclosure, *Journal of Acoustical Society of America* 88 (1990) 1993–2000.

[4] V. Martin, A. Bodrero, An introduction to the control of sound fields by optimising impedance locations on the wall of an acoustic cavity, *Journal of Sound and Vibration* 204 (1997) 331–357.

[5] P. Jean, Coupling integral and geometrical representations for vibro-acoustical problems, *Journal of Sound and Vibration* 224 (1999) 475–487.

[6] J. Martin, D. Van Maercke, J.P. Vian, Binaural simulation of concert halls: a new approach for the binaural reverberation process, *Journal of Acoustical Society of America* 94 (6) (1993) 3255–3264.

[7] J.L. Barbry, Technique des images et des rayons (locaux vides), *Les Notes Scientifiques et Techniques de l'INRS* 51 (1984).

[8] H. Kuttruff, *Rooms Acoustics*, 3rd Edition, E & FN Spon, London, 1991.

[9] M. Vorländer, Simulation of the transient and steady-state sound propagation in rooms using a new combined ray-tracing/image-source algorithm, *Journal of Acoustical Society of America* 86 (1989) 172–178.

[10] P.M. Morse, K.U. Ingard, *Theoretical Acoustics*, Princeton University Press, Princeton, NJ, 1986 (McGraw-Hill, New York, 1968).

[11] A.R. Wenzel, Propagation of waves along an impedance boundary, *Journal of Acoustical Society of America* 55 (1974) 956–963.

[12] J.B. Allen, D.A. Berkley, Image method for efficiently simulating small-room acoustics, *Journal of Acoustical Society of America* 65 (1979) 943–950.